Comprehensive models of novae at metallicity $Z = 0.02$ and $Z = 10^{-4}$

Hai-Liang Chen,[1,2,3,4]⋆ T. E. Woods,[5] L. R. Yungelson,[6] Luciano Piersanti,[8,9] M. Gilfanov,[2,7,10] and Zhanwen Han[1,3,4]

[1]*Yunnan Observatories, Chinese Academy of Sciences, Kunming, 650011,China*
[2]*Max Planck Institute for Astrophysics, Karl-Schwarzschild-Str. 1, Garching b. München 85741, Germany*
[3]*Key Laboratory for the Structure and Evolution of Celestial Objects, Chinese Academy of Sciences, Kunming 650011, China*
[4]*Center for Astronomical Mega-Science, Chinese Academy of Science, Beijing 100012, China*
[5]*Institute of Gravitational Wave Astronomy and School of Physics and Astronomy, University of Birmingham, Edgbaston, Birmingham B15 2TT, United Kingdom*
[6]*Institute of Astronomy, RAS, 48 Pyatnitskaya Str., 119017 Moscow, Russia*
[7]*Space Research Institute of Russian Academy of Sciences, Profsoyuznaya 84/32, 117997 Moscow, Russia*
[8]*INAF – Osservatorio Astronomico d'Abruzzo, via Mentore Maggini, snc, I-64100, Teramo, Italy*
[9]*INFN – Sezione di Perugia, via Pascoli, Perugia, Italy*
[10] *Kazan Federal University, Kremlevskaya str. 18, 420008 Kazan, Russia*

arXiv:1909.07643v2 [astro-ph.SR] 19 Sep 2019

Accepted XXX. Received YYY; in original form ZZZ

ABSTRACT

Novae are the observational manifestations of thermonuclear runaways on the surface of accreting white dwarfs (WDs). Although novae are an ubiquitous phenomenon, their properties at low metallicity are not well understood. Using the publicly-available stellar evolution code Modules for Experiments in Stellar Astrophysics (MESA), we model the evolution of accreting carbon-oxygen WDs and consider models which accrete matter with metallicity Z=0.02 or 10^{-4}. We consider both models without mixing and with matter enriched by CO-elements assuming that mixing occurs in the process of accretion (with mixing fraction 0.25). We present and contrast ignition mass, ejected mass, recurrence period and maximum luminosity of novae for different WD masses and accretion rates for these metallicities and mixing cases. We find that models with Z = 0.02 have ignition masses and recurrence periods smaller than models with low Z, while the ejected mass and maximum luminosity are larger. Retention efficiency during novae outbursts decreases with increasing metallicity. In our implementation, inclusion of mixing at the H/He interface reduces accreted mass, ejected mass and recurrence period as compared to the no-mixing case, while the maximum luminosity becomes larger. Retention efficiency is significantly reduced, becoming negative in most of our models. For ease of use, we provide a tabular summary of our results.

Key words: binaries:close - novae,cataclysmic variables - white dwarf - population II

1 INTRODUCTION

It is well established that novae occur in binaries hosting accreting white dwarfs, if the accretion rate is lower than a critical threshold (see, e.g., Warner 2003, and references therein). Accreted matter is compressed at the bottom of the envelope, leading to an increase in temperature. Eventually nuclear hydrogen burning is ignited in the degenerate matter, leading to a thermonuclear runaway (TNR). This is observable as a nova if the outburst results in mass loss.

On evolutionary timescales, all nova outbursts recur (Paczynski & Zytkow 1978). If the accretion rate is larger than a critical value, there is a regime in which hydrogen may burn stably in the envelope of the WD. If, however, the accretion rate is larger than the maximum stable burning rate, then no hydrostatic solutions are possible for a thin burning shell (see discussion in Shen & Bildsten 2007). In this case, the ensuing evolution remains uncertain. A number of studies (e.g., Nomoto et al. 1979; Iben 1988; Cassisi et al. 1998) have found that, at such high accretion rates and nuclear-burning luminosities, the WD envelope will expand to red giant dimensions. Hachisu et al. (1996) argued, however, that a peak in the opacity due to iron will lead to an optically thick wind, moderating the accretion rate and preventing significant expansion of the WD envelope.

Novae have been observed in the disk and bulge of the Galaxy and in external galaxies of different morphological types (see, e.g., Shafter et al. 2014; Shafter 2017), as well as in Galactic and extragalactic globular clusters (see, e.g., Shara & Drissen 1995; Kato et al. 2013; Curtin et al. 2015, and references therein). Novae in different populations exhibit different characteristics. This may be interpreted as a consequence of a dependence of the masses of WDs and their companions on the metallicity (e.g., Umeda et al. 1999;

⋆ E-mail:chenhl@ynao.ac.cn

© 0000 The Authors

Doherty et al. 2015) and typical age of stellar populations (e.g., Della Valle 2002; Shafter et al. 2014).

A link between the properties of classical Novae and metallicity has long been established. Starrfield et al. (1978) found that substantial enrichment by carbon is necessary in order to release sufficient energy for the rapid ejection of matter, while enrichment of accreted envelopes by β^+ unstable isotopes, which decay and release energy, facilitates mass ejection (see also Starrfield et al. 2016, for the latest review). Through the opacity, metallicity also influences the amount of energy retained in the burning layer, and hence the rate of temperature growth and the amount of ejected mass. As well, the light-curves of Novae have been shown to become slower with decreasing metallicity (Kato 1997; Kato et al. 2013). Observationally, it was discovered that "all novae for which reasonable abundance data are available appear to be enriched in either helium or heavy elements, or both", while the presence of Ne, Na, Mg, and Al in ejecta suggested the existence of ONe accretors (Truran & Livio 1986). From these observations and model data it was inferred that matter in the burning layers of novae is enriched by the matter from the cores of WDs.

Several 2D and 3D simulations of TNR (e.g. Glasner & Livne 1995; Casanova et al. 2010, 2016, 2018; Glasner et al. 2012; José 2014; Starrfield et al. 2017) have demonstrated that Kelvin-Helmholtz instabilities arising when a TNR has already fully developed can lead to enrichment of the envelope to levels consistent with observations. Motivated by these studies, Denissenkov et al. (2013) applied a convective boundary mixing algorithm implemented in the 1-D stellar evolution code MESA, and succeeded in reproducing an enhancement of metal abundances in the ejected matter up to $Z = 0.29$ for a 1.20 $M_\odot$ CO WD, commensurate with observed values. 2D simulations by Glasner et al. (2012) and Casanova et al. (2016, 2018) have shown that the mixing process may depend on the WD composition. In particular, in ONeMg WDs the scale of mixing is larger than in CO WD, leading to more energetic outbursts. It should be noted that these 2D and 3D simulations have only been carried out for a quite limited number of combinations of WD masses and accretion rates.

In hydrodynamic studies (Prialnik 1987), it was found that mass loss over the course of a full Nova eruption cycle is driven by dynamical acceleration of the matter leading to shock-ejection, followed by phases of continuous mass loss via optically thick winds and nebular mass-loss. Mass loss terminates when the mass of the envelope declines below a critical limit and nuclear burning is extinguished (Fujimoto 1982). In hydrostatic computations similar to the present study, approximations to this mechanism are applied, such as mass loss by opacity-peak-driven optically thick sub-Eddington winds (e.g., Kato 1997), optically thick radiatively driven super-Eddington winds (SEW) (Shaviv 2002), mass-loss via common envelope (e.g., Livio et al. 1990) or loss of all expanding WD matter that crosses the Roche lobe radius (e.g., Wolf et al. 2013). Ultimately, understanding which of these processes (or what combinations) are principally responsible for driving mass loss must be informed by future observations.

It was speculated already in early studies (e.g., Schatzman 1963; Truran & Cameron 1971; Fujimoto & Taam 1982; MacDonald 1984; Prialnik 1986; Starrfield et al. 1988) that WDs experiencing nova outbursts may retain a fraction of accreted matter and ultimately grow to become the progenitors of type Ia supernovae (SNe Ia) upon reaching the Chandrasekhar mass limit. The fraction of accreted matter which is not ejected by novae is referred to as the retention efficiency, defined as

$$\eta = \frac{M_{\rm acc}^{tot} - M_{\rm ej}}{M_{\rm acc}^{tot}}, \quad (1)$$

where $M_{\rm acc}^{tot}$ is the mass accreted by a WD over a single nova cycle, and $M_{\rm ej}$ is the ejected mass. Note that η may be negative, if the WD is eroded as a result of an outburst.

Recent theoretical and observational efforts have placed strong limits on the amount of matter which may be accumulated by accreting WDs in the steady-burning regime, particularly in the context of SN Ia progenitors (e.g., Gilfanov & Bogdán 2010; Woods & Gilfanov 2014; Johansson et al. 2016; Denissenkov et al. 2017; Woods et al. 2017, 2018; Graur & Woods 2019; Kuuttila et al. 2019). The contribution of accreting WDs in the nova regime has also been strongly constrained for metallicities typical of the local Universe (see e.g., Soraisam & Gilfanov 2015), however relatively little is known for the low metallicity case. In particular, improving our understanding of the mass retention efficiency remains a critical issue (see, e.g. Bours et al. 2013; Maoz et al. 2014; Postnov & Yungelson 2014).

The retention efficiency may be expected to be higher in low-Z environments, since the opacity of stellar matter (which sets the pace of mass-loss) is then lower, and the effects of expansion due to radiation pressure are smaller. Piersanti et al. (2000) have investigated the evolution of low-mass accreting WDs ($M_{\rm WD} \leqslant 0.68\,M_\odot$) with metallicities $Z = 0.02, 10^{-3}, 10^{-4}$. They found that at low metallicity hydrogen may burn stably at lower accretion rates than at solar metallicity, and the mass necessary for a TNR at a given $\dot{M}$ is larger than for solar metallicity. The latter result was confirmed by subsequent studies (Starrfield et al. 2000; José et al. 2007; Shen & Bildsten 2007) who studied accretion onto more massive WDs for a range of sub-solar metallicities.

The aim of this paper is to systematically study the characteristics of novae at approximately solar and very low metallicity, and thereby draw conclusions on the influence of metallicity on nova properties. We also investigate the significance of enrichment of the accreted H-rich layer by the matter from the underlying CO-core ("mixing"). In this work, we are primarily interested in the conditions for steady burning of hydrogen at the surface of accreting WDs, the amount of mass to be accreted to trigger an outburst, and in the amount of mass eventually ejected. This is motivated by our eventual goal of modelling of nova populations in different environments, and determining the precursors of SNe Ia.

For this work, we calculated a grid of accreting CO WD models for a range of masses $M_{\rm WD} = 0.51 - 1.30\,M_\odot$, accretion rates $\dot{M} = 10^{-10} - 10^{-6}\,M_\odot\,{\rm yr}^{-1}$, and metallicities $Z = 0.02, 10^{-4}$. These two values of Z may be considered representative of metal-rich and metal-poor environments. For both values of Z, we consider models with a simplified mixing approximation and without it.

The paper is structured as follows. In Section 2, we describe the approach we used to obtain initial WD models, and our assumptions in modelling the evolution of accreting WDs. In Section 3, we present our results for the "steady burning strip", describe in detail a full nova cycle at low metallicity and its differences with a cycle for high Z, and present physical characteristics of Novae at metallicities $Z = 0.02$ and $Z = 10^{-4}$. Uncertainties and implications of our results are addressed in Section 4. Finally, we summarise our results and conclude in Section 5.

2 SIMULATION ASSUMPTIONS

2.1 Initial WD models

In our study, we use the stellar evolution code *Modules for Experiments in Stellar Evolution* (MESA version 4906; Paxton et al. 2011, 2013, 2015)[1]. To obtain the initial WD models, we evolve stars with different initial masses and different metallicities, from the Zero-Age Main-Sequence to the Asymptotic Giant Branch, halting at the stage when the stellar CO-core mass is close to the desired WD mass. At that point, we impose a very high mass loss rate to remove the envelopes of the stars. This is the canonical approach adopted by many previous studies (Denissenkov et al. 2013; Ma et al. 2013; Wolf et al. 2013; Wang 2018).

In this way, we produce CO WDs models with mass M = 0.51, 0.60, 0.70, 0.80, 0.90, 1.00 $M_\odot$. For CO WDs with mass $M > 1.00\ M_\odot$, we make WD models by allowing a 1.0 $M_\odot$ WD to accrete C/O matter until its total mass reaches 1.10 $M_\odot$, 1.20 $M_\odot$, or 1.30 $M_\odot$. In this work, we do not explore ONe WD models. This is because, after reconsideration of observational data, Livio & Truran (1994) found that the fraction of novae with ONe WDs may be much lower than previously suggested. More recently, Chen et al. (2016) obtained a similar conclusion from their population synthesis study.

After each initial WD model was produced, it was allowed to cool to a lower temperature. Townsley & Bildsten (2004) found that the equilibrium core temperatures of WDs in typical cataclysmic variables are below 10^7 K. In addition, Chen et al. (2016) found that the low temperature models from Yaron et al. (2005) are preferred when compared to observational data of novae in the M31 galaxy. Here we neglect the possible effect of H/He shells on the cooling of WDs and their central temperatures. We assume the WD central temperature to be 10^7 K and cool every initial white dwarf model until its central temperature becomes very close to this value. The initial WD models have a thin He and H shell on their surface. The H shell masses are between $10^{-6} - 10^{-4}\ M_\odot$ and the He shell masses are between $10^{-4} - 10^{-2}\ M_\odot$.

2.2 Nova outburst calculation

To simulate nova outbursts, we follow the evolution of models using MESA for different combinations of initial WD mass and fixed accretion rate. We have computed nova models with metallicities $Z = 0.02$ and 10^{-4} and mixing fractions 0.0 ("no mixing case") and 0.25 ("mixing case"). In order to better understand the dependence of nova properties on metallicity, we have also computed several models with metallicities ranging from $Z = 10^{-5}$ to $Z = 0.08$ (see Figs. 7, 10 below). For any given metallicity Z, the hydrogen mass fraction is computed as $X = 0.76 - 3.0Z$, $Y = 0.24 + 2.0Z$; note that $\Delta Y/\Delta Z$=2 is appropriate for abundances from primordial to solar (Pols et al. 1998). Initial relative abundances of different isotopes in the matter were implemented following Lodders (2003). In our study, we model mass accretion rates ranging from 10^{-10} $M_\odot$ yr^{-1} to 10^{-6} $M_\odot$ yr^{-1}. We did not consider accretion rates lower than 10^{-10} $M_\odot$ yr^{-1}, as such accretion rates correspond to CVs that have evolved beyond the period minimum (they have "bounced"). Though several novae with orbital periods between about 2 hr and 80 min are known (Ritter & Kolb 2011), it is hard to identify their evolutionary stage. While extant models predict the possibility of novae among bouncers (Yaron et al. 2005), they are certainly rare, due to their long recurrence periods, and therefore hardly contribute to the statistics of observed novae (Chen et al. 2016).

In our calculations, we do not consider the rotation of WDs and convective overshooting. Given that mixing processes cannot be investigated self-consistently in 1D stellar models, we do not include mixing with the core via a physical mechanism. Instead, following Politano et al. (1995), we assume that accreted matter is enriched in C, O, and Ne. The enrichment (mixing fraction) may be constrained by observations of the abundances of heavy elements in the ejecta of novae. However, it is well known that estimates of the metallicities of the latter might be rather uncertain (e.g. Gehrz et al. (1998); Kelly et al. (2013); see also Jose and Shore in Bode & Evans (2008).) Even for the same nova, abundances derived from different observations can vary by a factor of several. Motivated by this circumstance, Kelly et al. (2013) proposed using the line ratios ΣCNO/H, Ne/H, Mg/H, Al/H and Si/H as measures of the mixing fraction, and found that the latter should be $\leqslant 0.25$ (by mass). Note, however, that Kelly et al. (2013) focused on ONe WDs only and the latter have greater mixing compared to CO WDs (Casanova et al. 2018). Therefore, a mixing fraction of 0.25 can be taken as an upper limit for CO WDs. We use this value of the mixing fraction in our calculations in order to test the maximum effect that mixing may have upon nova explosions. It is worth noting, however, that the mixing fraction should depend on the WD mass and accretion rate.

In models with mixing, the accreted matter is enriched in CNO cycle catalysts. In principle, the abundances of matter in the underlying white dwarfs should depend on their progenitor mass, the white dwarf mass itself, overshooting, and mass loss during the preceding evolution. Here, however, we make the simplifying assumption of neglecting the differing chemical abundances among WDs of differing masses, and assume that the chemical composition of all underlying white dwarfs is $X(^{12}\mathrm{C}) = 0.41$, $X(^{16}\mathrm{O}) = 0.57$, $X(^{22}\mathrm{Ne}) = 0.02$ for $Z = 0.02$ models and $X(^{12}\mathrm{C}) = 0.6354$, $X(^{16}\mathrm{O}) = 0.3645$, $X(^{22}\mathrm{Ne}) = 10^{-4}$ for $Z = 10^{-4}$ models. As a sanity check for this assumption, we computed toy models with $X(^{12}\mathrm{C}) = 0.88$, $X(^{16}\mathrm{O}) = 0.10$, $X(^{22}\mathrm{Ne}) = 0.02$ and $X(^{12}\mathrm{C}) = 0.10$, $X(^{16}\mathrm{O}) = 0.88$, $X(^{22}\mathrm{Ne}) = 0.02$. Our results (together with those for our "standard" model) are presented in Table 1. They agree with the inference of Hernanz et al. (1996) that the abundance of ^{12}C is crucial for the development of a TNR, which develops more rapidly and has lower $M_{\rm ign}$ with increasing ^{12}C in the accreted matter (see also, e.g., Starrfield et al. 2017). However, the difference in $M_{\rm ign}$ and $M_{\rm ej}$ between the extreme cases does not exceed about 30% and is $\leqslant 16\%$ for L_{max}. This difference cannot be considered significant given the present uncertainties in modeling novae.

We use the MESA nuclear network `cno_extras_o18_to_mg26_plus_fe56`, which includes 29 isotopes, from H to ^{26}Mg and ^{56}Fe, linked by 75 nuclear processes. This network is based on the one derived by Wolf et al. (2013) and includes *pp* and *pep* chains, as well as cold and hot CNO

Table 1. Comparison of models with different enrichment of accreted matter. Masses are in $M_\odot$.

$M_{\rm WD}$	$X(^{12}\mathrm{C})$	$X(^{16}\mathrm{O})$	$M_{\rm ign}$	$M_{\rm ej}$	$L_{\rm max}/L_\odot$
0.51	0.41	0.57	$1.05\cdot10^{-4}$	$9.67\cdot10^{-5}$	$4.22\cdot10^{4}$
0.51	0.88	0.10	$8.67\cdot10^{-5}$	$7.85\cdot10^{-5}$	$4.09\cdot10^{4}$
0.51	0.10	0.88	$1.15\cdot10^{-4}$	$1.03\cdot10^{-4}$	$4.07\cdot10^{5}$
1.0	0.41	0.57	$1.25\cdot10^{-5}$	$1.19\cdot10^{-5}$	$1.24\cdot10^{4}$
1.0	0.88	0.10	$1.16\cdot10^{-5}$	$1.15\cdot10^{-5}$	$1.16\cdot10^{4}$
1.0	0.10	0.88	$1.34\cdot10^{-5}$	$1.30\cdot10^{-5}$	$1.34\cdot10^{4}$

[1] MESA web page: `http://mesa.sourceforge.net`.

and NeNa cycles. It represents the minimum network needed to accurately evaluate the energy delivered by nuclear burning during a full nova cycle and, hence, it allows the correct determination of the physical evolution of an accreting CO WD.[2]

In MESA, an adaptive grid method for spatial discretization is used. As a compromise between numerical accuracy and computational time, in the inner part of the model where Lagrangian coordinates are used, we determine the number of grid points using the criterion `mesh_delta_coeff = 0.25`. This increases the number of mesh-points by a factor close to 4, compared to the number set by default; in the outer part of the model, where the cell size is defined as a fraction of the total mass (dq), we increased the number of grid points by setting `max_surface_cell_dq = 1d-12`. With these values, the typical number of zones in our model is around $6 \times 10^3 - 10^4$. In order to verify that our choice of mass grid does not introduce an artificial mixing at the boundaries between regions with different chemical composition, thus producing inaccurate results, we performed test calculations for M_{WD}=1 $M_\odot$and $\dot{M}$=10^{-8} $M_\odot$/yr with `mesh_delta_coeff = 1.0`, `max_surface_cell_dq = 1d-12` and `mesh_delta_coeff = 0.25`, `max_surface_cell_dq = 1d-10`. Variations of accreted mass prior to outburst and ejected mass did not exceed 12%, while the recurrence time between the outbursts changed by less than 8% and $\log L_{max}$ varied by only 0.01.

Mass loss rates during outbursts are computed using the default prescription given in MESA, super-Eddington wind (SEW):

$$\dot{M} = -2\frac{L - L_{\rm edd}}{v_{\rm esc}^2}, \qquad L_{\rm edd} = \frac{4\pi GMc}{\overline{\kappa}}, \tag{2}$$

where $v_{\rm esc}$ is the escape velocity at the photosphere of the accreting WD, $L_{\rm edd}$ is the Eddington luminosity and $\overline{\kappa}$ is the mass-weighted-mean Rosseland opacity of the outer layers of the WD (optical depth $\leqslant 100$).[3] Equation (2) is inspired by the finding that energy injection slightly below the point where the local escape velocity exceeds the sonic speed may drive super-Eddington winds (Quinn & Paczynski 1985; Paczynski & Proszynski 1986; Shaviv 2002); see also, e.g., Quataert et al. (2016) for a more recent discussion. We will discuss the influence of the mass loss prescription on our results in greater detail in 4.4.

In an effort to assess the steady-state behaviour of novae (i.e., after many outbursts), in our MESA calculations we follow the evolution of each accreting WD through $\simeq 1 - 100$ novae outbursts, depending principally on the convergence of each accreting white dwarf model.

3 RESULTS

3.1 Steady burning regime

In Fig. 1, we show the limits of the steady-state burning regimes for models of accreting WD with $Z = 0.02$ and $Z = 10^{-4}$ and without mixing. The data on these boundaries in our calculations are presented in Tables A1 and A2. Fitting formulae for the boundaries are also provided in Appendix A. In the steady-state H-burning regime, the bolometric luminosity of a WD remains constant. Accreting WDs with accretion rates larger than the maximum steady-burning rate greatly expand, while in the steady-burning regime their radii do not increase significantly. Below the lower boundary, H-burning is unstable and the bolometric luminosity experiences quasi-regular oscillations (Paczynski & Zytkow 1978; Iben 1982, see also Fig.1 in Ma et al. 2013). As is well known, there is no gradual transition between stable and unstable burning, i.e., flashes appear below the limiting accretion rate with non-zero amplitude. The plot shows that the steady burning boundary is lower at lower metallicity. The reason for this is straightforward: the limits for steady burning are determined by the requirement that H-burning energy balances the radiative losses from the surface along the high luminosity branch in the HRD-loop (see e.g. Piersanti et al. 2000). As the luminosity level of this branch depends mainly on the mass of the CO core underlying the burning shell, it is about the same for all metallicities. For lower metallicity, however, the CNO abundance in the models without mixing is lower, leading to a lower H-burning rate. On the other hand, the condition for the steady burning regime is that the accretion rate is equal to the H-burning rate. This explains why the limits of the steady burning regime are located at lower values of $\dot{M}$ for lower Z.

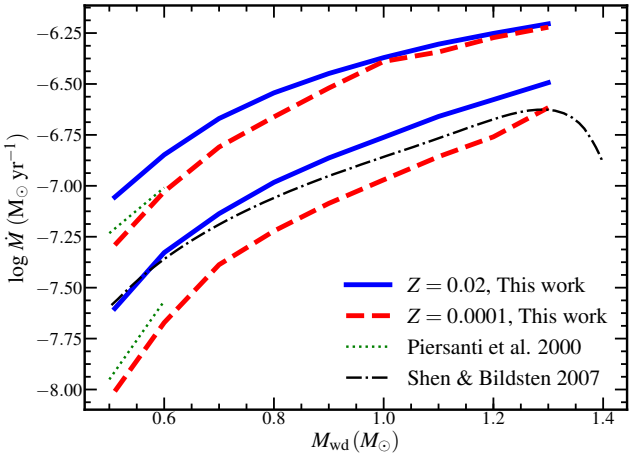


Figure 1. Steady burning regimes for $Z = 0.02$ (blue thick solid line) and $Z = 10^{-4}$ (red thick lines) for our models without mixing in the M_{WD}-$\dot{M}$ plane. The thin dotted line represents the steady burning regime for $Z = 10^{-4}$ from Piersanti et al. (2000) and the thin dash-dotted line represents the lower boundary of the steady burning regime for $Z = 10^{-4}$ from Shen & Bildsten (2007). The data and fitting formulae of these boundaries from our calculation are presented in Appendix A.

In Fig. 1, we also compare our results for the steady burning regimes at $Z = 10^{-4}$ with previous studies. Note that Piersanti et al. (2000) considered only low mass WDs and Shen & Bildsten (2007) present only the lower boundary of the steady burning regime for $Z = 10^{-4}$. Our results are consistent with the results of Piersanti et al. (2000). The lower boundary of the steady burning regime in this work, however, is below that obtained by Shen & Bildsten (2007). This is mainly due to the fact that Shen & Bildsten (2007) adopted a one-zone approximation, in which the properties of the H-shell are defined at the bottom of the shell, while the maximum of energy generation occurs at larger Lagrangian coordinate. Given

[2] We note that this network does not include the MgAl cycle, active for temperatures above $\sim 2.5 \times 10^8$ K; this cycle is important for deriving the nucleosynthesic yield, but provides a negligible contribution to the nuclear energy production.

[3] A test run for M_{WD}=1.2 $M_\odot$, $\dot{M} = 10^{-8}$ $M_\odot$yr^{-1} has shown that variation of this optical depth from $\tau = 100$ to $\tau = 30$ resulted in an increase of the accreted mass prior to ignition by about 8% and the ejected mass by only $\simeq$11%, i.e., the dependence on the actual optical depth over which the opacity is averaged does not have a substantial effect.

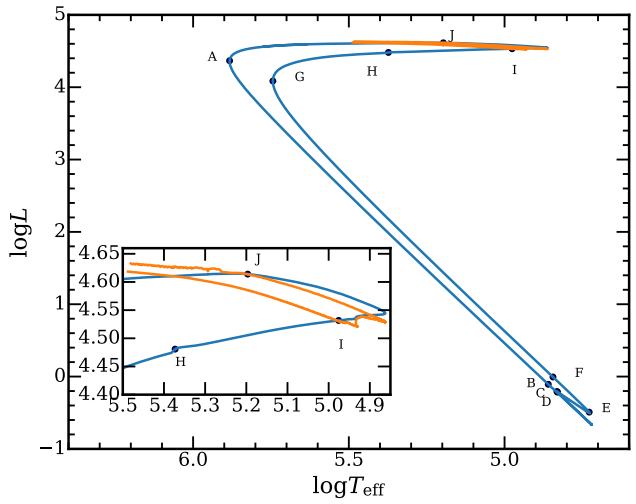


Figure 2. Evolution of the model with M_{WD}=1.20$M_\odot$, $\dot{M}$=10^{-9} $M_\odot yr^{-1}$ and Z=10^{-4} in the HR diagram for the no-mixing case. Along the track some relevant epochs are marked by capital letters: **A**: bluest point along the loop; **B**: minimum temperature of the H-burning shell; **C**: full ignition of H-burning via CNO cycle; **D**: flash-driven convection sets in; **E**: convective shell attains the surface; **F**: maximum luminosity of the H-burning shell; **G**: maximum temperature of the H-burning shell; **H**: convective shell recedes from the surface; **I**: onset of mass loss via super-Eddington wind; **J**: end of the mass loss episode. Orange line shows the behaviour of L_{Edd} close to and during mass-loss stage.

that a part of the nuclear burning energy can be absorbed by the accreted H-layer itself and massive WDs have thinner H-layers, less energy will be absorbed. This is why the discrepancy for massive WDs is smaller.

3.2 Evolution of the physical properties of an accreting WD during a full Nova cycle

The evolution of H-accreting WDs via recurrent flashes has been addressed by many authors in the past. WDs are known to evolve along closed loops in the HR diagram, as displayed in Fig. 2 where we report one nova outburst we computed for the model with CO WD mass M_{WD}=1.20 $M_\odot$, accretion rate $\dot{M}$=10^{-9} $M_\odot$ $yr^{-1}$and metallicity Z=10^{-4} for the no-mixing case. In this figure, several important epochs in the evolution along the loop in the HRD are annotated by letters. Physical properties of the WD at these epochs are presented in Table 2.

At the epoch corresponding to the bluest point of the track (point **A** in Fig. 2), the H-burning shell is no longer able to provide the energy to balance the radiative losses from the surface (see discussion in Iben 1982), so that the luminosity of the WD decreases, the external layers contract and the model evolves along the cooling sequence. During the following phase, lasting for $\Delta t_{AB} = 1558.63$ yr, mass deposition determines the compressional heating of the H-rich mantle, even if the delivered energy is not able to counterbalance the radiative losses and the H-burning shell progressively cools down (see right panel in Fig. 3). The energy contribution coming from the CNO cycle rapidly extinguishes, even if H-burning never completely dies, as *pp* and *pep* reactions are always active as well as *p*-capture on ^{12}C (see right panel in Fig 3). Due to the combined action of fresh matter accretion and contraction of the H-rich mantle, at the epoch **B** in Fig. 2, the H-burning shell ceases cooling down, while the local density continuously increases. As the H-rich layer grows in mass, the temperature of the H-burning shell T_H progressively increases and, when it attains $\sim 3.7 \times 10^7$ K after $\Delta t_{BC} = 33900.45$ yr, the CNO cycle is fully active[4]. Due to the partial degeneracy of the matter at the H-burning shell and the continuous mass deposition, the local energy production largely increases and after $\Delta t_{CD} = 27.34$ yr convection sets in, because the timescale in which nuclear energy is delivered is shorter than the local thermal diffusion timescale, and in $\Delta t_{DE} = 5.50$ yr the flash-driven convective shell attains the surface of the accreting WD. The resulting H-flash turns into a thermonuclear runaway which drives the evolution toward higher luminosity and larger effective temperature until, after $\Delta t_{EF} = 5.26$ hr the H-burning luminosity attains a maximum, though the temperature in the burning shell still continues to rise for $\Delta t_{FG} = 4.24$ day. When the model attains a surface luminosity of $\sim 10^4 L_\odot$, it evolves redward at almost constant luminosity. After $\Delta t_{GH} = 14.8$ day, convection starts to recede from the surface, but the star still expands, evolving redward. During this phase, the surface luminosity becomes larger than the Eddington limit after $\Delta t_{HI} = 49.3$ day, and mass loss via stellar wind begins.

When the large energy excess produced by the thermonuclear runaway has been dissipated via both mechanical work to expand the H-rich mantle and stellar wind mass loss, the H-burning shell moves outward in mass rapidly converting hydrogen into helium. The reduction of the H-rich mantle via mass loss and nuclear burning determines the blue-ward evolution of the model up to when, after $\Delta t_{IJ} = 1.423$ yr, mass loss ceases. It is worth noticing that during the mass loss phase the Eddington luminosity progressively increases, due to a decrease of the average opacity in the envelope $\overline{\kappa}$ (see the inside panel in Fig. 2). At epoch **J** the energy production via H-burning almost completely counterbalances the radiative losses from the surface; the additional energy contribution comes from the contraction of the H-rich mantle. As the star consumes hydrogen, the energetic contribution of nuclear burning decreases and that of the contraction increases. The latter determines the blue-ward evolution of the WD. When the gravitational energy release exceeds ∼5% of the total released energy, the star attains the bluest point in the HR diagram and H-burning rapidly declines.

This general scenario is valid also for high metallicity models, even if some important differences exist. First, as the CNO abundance in the accreted matter is larger, H-burning is ignited sooner, at lower T_H; this implies that a lower mass has to be accreted in order to trigger the TNR and, hence, the degeneracy level at the H-burning shell is lower (slightly lower ignition density – see Table 2). It has to be remarked also that, due to the larger CNO abundance in the $Z = 2 \times 10^{-2}$ model, the CNO cycle provides an energy contribution comparable to that from the *pp*-chain. The reduced degeneracy at the H-burning shell and the larger CNO abundance in high metallicity models act in opposite directions, the latter causing a stronger H-flash, the former allowing a larger outward flux of thermal energy produced during the H-flash and, hence, a less rapid increase of the local temperature. We found that in the Z=2×10^{-2} case L_H^{max} is larger while T_H^{max} is lower as compared to the Z=10^{-4} one (see Table 2). Notwithstanding, the maximum surface luminosity during the loop is quite similar, while the percentage of the mass transferred during the full nova cycle effectively retained by

[4] We assume that CNO is fully active when its contribution to the total surface luminosity is 10 times that due to the *pp* chain. Note that at this epoch the mass fraction abundance of ^{16}O at the H-burning shell has already been reduced by ∼5%.

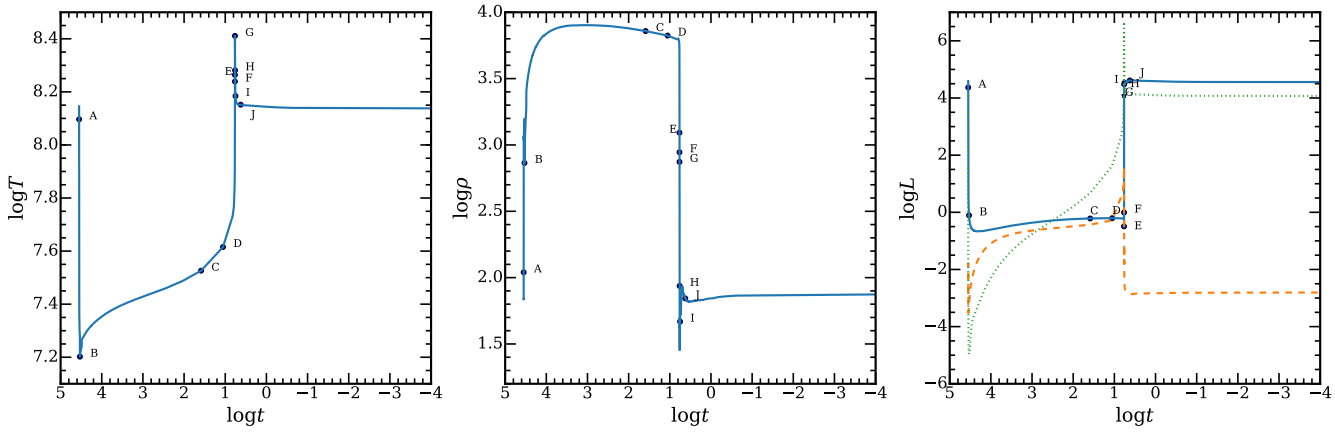


Figure 3. Time (remaining time of nova cycle) evolution of temperature (left panel) and density (middle panel) at H-burning shell for the same model as in Fig. 2. In the right panel we report the luminosity at the H-burning shell due to the *pp*-chain (dashed line) and CNO cycle (dotted line). For comparison we report also the total surface luminosity (solid line). Points and letters along the curves mark the same epochs displayed in Fig. 2 and in Table 2. Time is in yr.

Table 2. Physical properties of the models with M_{WD}=1.20$M_\odot$, $\dot{M}$=$10^{-9}$$M_\odot$yr^{-1}for the no-mixing case. The letters in the first row refer to the epochs marked in Fig. 2. We list: Δt – the time elapsed from the previous epoch in yr (for epoch **A** it is 0); ΔM_{acc} – the amount of mass accreted from epoch **A** (in 10^{-5} $M_\odot$); $\log(L_H/L_\odot)$ – the H-burning luminosity at the H-burning shell; ρ_H – the density (in g$\cdot$cm^{-3}) and T_H – the temperature (in K) at the H-burning shell; $\log(L/L_\odot)$ – the surface luminosity; $\log T_{eff}$ – the effective temperature (in K). The upper part of the table refers to the models accreting matter with Z=10^{-4}, while the lower part — to models with Z=2×10^{-2}.

	A	**B**	**C**	**D**	**E**	**F**	**G**	**H**	**I**	**J**
					$Z=10^{-4}$					
Δt	0	1558.63	33900.45	27.34	5.50	0.0006	0.0116	0.0405	0.135	1.423
ΔM_{acc}	0	0.156	3.546	3.548	3.549	3.549	3.549	3.549	3.549	0.439
$\log(L_H/L_\odot)$	3.988	-0.153	-0.406	0.062	3.949	5.558	5.464	3.847	3.532	4.123
$\log\rho_H$	2.040	2.864	3.858	3.824	3.093	2.945	2.872	1.937	1.668	1.843
$\log T_H$	8.096	7.202	7.526	7.615	8.263	8.239	8.410	8.281	8.184	8.151
$\log(L/L_\odot)$	4.366	-0.107	-0.215	-0.206	-0.491	-0.005	4.085	4.480	4.531	4.614
$\log T_{eff}$	5.882	4.859	4.829	4.831	4.728	4.844	5.743	5.372	4.975	5.196
					$Z=2\times10^{-2}$					
Δt	0	941.18	18603.19	32.14	0.658	1.032e-5	6.520e-5	2.835e-4	3.765e-4	0.360
ΔM_{acc}	0	0.094	1.954	1.957	1.957	1.957	1.957	1.957	1.957	0.043
$\log(L_H/L_\odot)$	4.07	-0.86	-0.74	1.11	6.64	6.84	5.52	6.236	5.83	4.12
$\log\rho_H$	1.575	2.827	3.795	3.740	3.248	3.100	2.40	1.36	1.19	1.470
$\log T_H$	7.985	7.098	7.375	7.542	8.105	8.146	8.372	8.226	8.186	8.013
$\log(L/L_\odot)$	4.45	-0.68	-0.54	-0.53	-0.69	-0.72	3.795	4.458	4.47	4.57
$\log T_{eff}$	5.93	4.72	4.75	4.75	4.70	4.69	5.71	5.32	5.15	5.90

the accreting WD is in the former model $\sim 2\%$ and in the latter $\sim 12\%$, respectively. Such an occurrence is, once again, a direct consequence of the different metallicity, the Z=0.02 model having a larger thermal content per unit mass in the H-rich mantle. In addition, the surface opacity is also larger so that the corresponding Eddington luminosity is lower and, hence, in our computations mass loss starts when the model is more compact with respect to the $Z=10^{-4}$ case (see Tab. 2). This implies that in the high metallicity model a very small amount of the energy delivered via nuclear burning is employed to expand the model before the onset of super-Eddington wind mass loss and, hence, a larger portion of the accreted matter is expected to be lost.

Another important aspect related to the metal content (i.e. CNO abundance) of the accreted matter is the abundance of the β-unstable isotopes ^{13}N, ^{14,15}O, and ^{17}F in the convective envelope of the accreting WD. These isotopes are produced by the hot CNO cycles and, since they have a longer *p*-capture timescale with respect to the convective mixing timescale, they are carried outward by convection. Then, their local decay into their daughter nuclei ^{13}C, ^{15}N, and ^{17}O provides additional power to trigger the expansion and the ejection phase. In our models, as the maximum attained temperatures during the outbursts are quite similar (see Table 2), the amount of β-unstable isotopes dredged up to the surface scales as the total metallicity, being larger at Z=0.02.

In Fig. 4, we show the evolution of ignition mass and ejected mass for multiple nova outbursts in the initial stage of our calculations, while models attain a steady-state pattern of outbursts, for M_{WD}= 1.00 $M_\odot$, accretion rate $\dot{M}_{accr}$= 10^{-8} $M_\odot$/yr, $Z=0.02$ and no mixing. Ignition mass and ejected mass are defined as the amount of matter accreted and ejected during one full nova cycle, respectively (see above). In the following, we consider the properties of the last computed flash as typical for novae with given M_{WD} and $\dot{M}$.

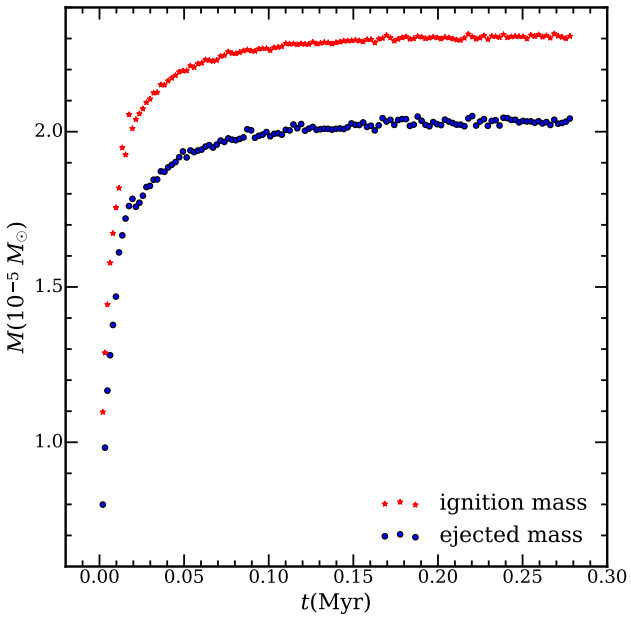


Figure 4. Evolution of ignition mass and ejected mass as a function of time from the onset of mass transfer for accreting WDs with M_{WD}= 1.00 $M_\odot$, accretion rate $\dot{M}_{accr}$= 10^{-8} $M_\odot$/yr, metallicity $Z = 0.02$ and without mixing.

3.3 Novae properties at metallicity $Z = 0.02$ and 10^{-4}

In Tables A3 and A4, we present characteristics of novae outbursts for the models with $Z = 0.02$ and $Z = 10^{-4}$ without mixing of accreted matter: accreted mass M_{acc}, ejected mass M_{ej}, and the maximum luminosity during the outburst L_{max}. The results for the models with mixing are presented in Tables A5 and A6. Recall that in the computations of these models the WDs accrete matter with enhanced C, O and Ne abundance (see 2.2). Physically, this procedure corresponds to the assumption that at each time step the accreted matter ΔM_{acc}, with Z being that of the donor, is instantaneously mixed with a fraction of the underlying C- and O-rich core corresponding to $\Delta M_{mix} = \frac{1}{3} \cdot \Delta M_{acc}$. As a consequence, the accreted matter progressively penetrates the underlying WD, which becomes gradually eroded. Thus, for the models with mixing and given a mixing fraction of 0.25, at the instant of ignition the total mass of the C- and O-enriched layer is

$$M_{ign}^{tot} = \int_{loop} (\dot{M}_{mix} + \dot{M}_{acc})dt = \int_{loop} \dot{M}_{acc}(1+\frac{1}{3})dt = \frac{4}{3}M_{acc}. \quad (3)$$

Equation (3) implies that in our calculations of the mixing case, the conditions for ignition are ultimately set by the amount of matter transferred from the donor, as in the no-mixing case.

In Fig. 5 we compare our models with $Z = 0.02$ and the models of Yaron et al. (2005). In making such a comparison, it is important to keep in mind the different numerical implementations, particularly the different prescriptions invoked for mass loss and for diffusion at the core/envelope interface, employed by Yaron et al. (2005).[5] Furthermore, in comparing Yaron et al. (2005) and our results it should be noted that while we take the "last" outburst as typical, Yaron et al. (2005) present characteristics of a random outburst; therefore a direct comparison may be misleading if in either case the steady state is not reached. Nevertheless, the values of M_{ign} and M_{ej} obtained in the no-mixing case for the $M_{WD} \leqslant 1\,M_\odot$ and $10^{-10} \leqslant \dot{M} \leqslant 10^{-8}\,M_\odot$ yr^{-1} models reasonably agree with the values from Yaron et al. (2005). This may mean that in this range of WD masses the timescale of diffusion exceeds (1-10) Myr and it does not influence the hydrogen ignition process. Intersection of lines for these parameters may be attributed to numerical noise. We cannot draw a definitive conclusion with respect to the behaviour of L_{max} for $\dot{M} \leqslant 10^{-9}\,M_\odot$/yr, since in our calculation, due to convergence problems, the steady-state was not reached. However, we note that the non-monotonic behaviour for L_{max} found by Yaron et al. (2005) for low $\dot{M}$ models may hint to the same circumstance. Generally, we would expect that, with decreasing $\dot{M}_{accr}$, the maximum luminosity would increase, since H-ignition occurs in more degenerate matter.

Compared to the models without mixing, in the models with mixing ignition masses, ejected masses, and recurrence periods[6] are lower, as expected for a higher initial abundance of ^{12}C, if mixing before the TNR is assumed. For the same reason, the maximum luminosity is larger in these models (as long as we consider steady-state models). We note a relatively large difference between our results for mixing models and the results of Yaron et al., which is due to the larger degree of enrichment of the accreted layer by ^{12}C than may be enabled by diffusion.

Notably, among our models there are some with M_{ej}=0. Similar models have been found previously as well. In these models, the H-shell does not expand significantly during the outburst, leading to small photospheric radii and high effective temperatures. Therefore, these objects are likely to be bright in the extreme ultraviolet and supersoft X-rays, but faint in the optical band and difficult to observe (Shara et al. 1977; Fujimoto 1982; Ritter 1990). The supersoft X-ray source ASASSN-16oh was suggested as the first candidate for this kind of object (Hillman et al. 2019), but Maccarone et al. (2019) advanced an alternative interpretation, associated with the features of accretion onto WD for this X-ray source.

4 DISCUSSION

4.1 Influence of metallicity upon nova outbursts

Figure 6 presents a comparison of the properties of novae with $Z = 0.02$ and $Z = 10^{-4}$. A reduced abundance of CNO-elements results in a decrease in the opacity of the envelope matter, allowing more heat to leak out of compressed layers faster, leading to a slower increase of the temperature. As a result, more mass must be accreted prior to a TNR. The lower abundance of CNO-isotopes is balanced by a higher degree of degeneracy of the matter at the base of the H-shell and, hence, stronger outbursts and an even larger or comparable amount of ejected mass. However, this difference decreases with decreasing mass. In models with M_{WD}= 0.51 $M_\odot$ and M_{WD}= 0.60 $M_\odot$ and accretion rates $\dot{M} = 10^{-10}$ and 10^{-9} $M_\odot$ yr^{-1}, the luminosity during nova outbursts never exceeds

[5] For more details on their numerical method, see also Prialnik & Kovetz (1995).

[6] The recurrence period P_{rec} is the time elapsing between two successive epochs of maximum luminosity. It can be estimated as the ratio of the mass accreted during a full nova cycle over the accretion rate.

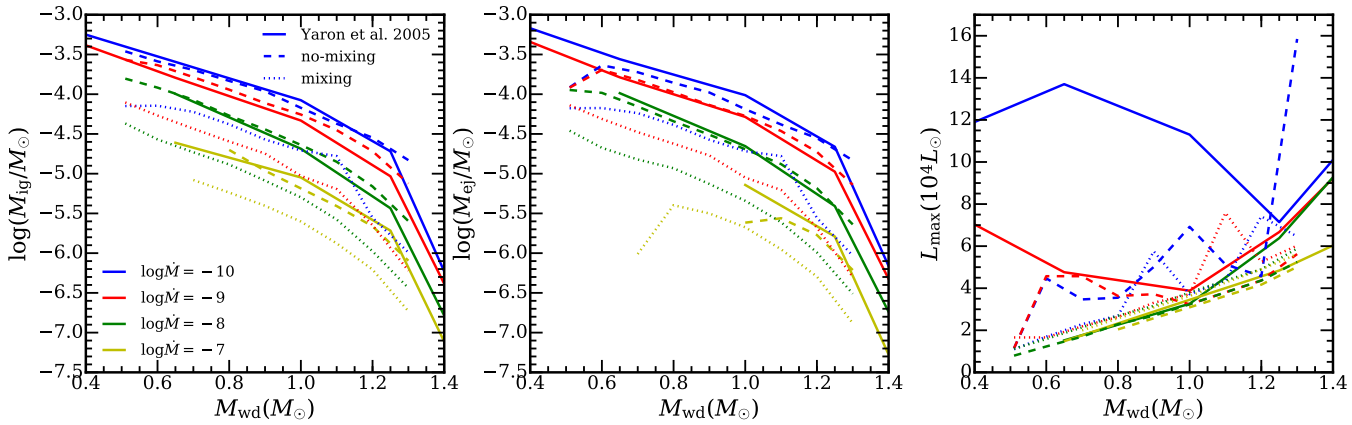


Figure 5. Comparison of ignition mass (left panel), ejected mass (middle panel) and maximum luminosity (right panel) for our models with $Z = 0.02$ with the results of Yaron et al. (2005). Note that convergence problems did not allow to compute enough outburst cycles for models with $\dot{M}_{\rm accr} = 10^{-10}\,M_\odot$/yr, leading to a large scatter in the right panel. Note, the models of M_{WD}=0.8, 0.9 $M_\odot$ accreting at the rate $10^{-7}\,M_\odot\ {\rm yr}^{-1}$ in no-mixing case do not eject matter.

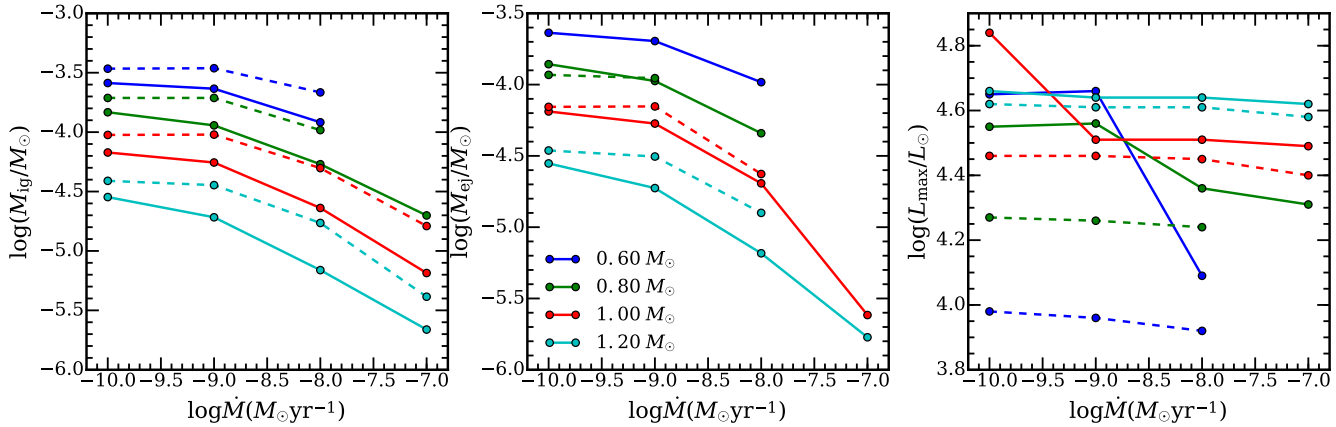


Figure 6. Comparison of novae properties for models without mixing, and metallicities $Z = 0.02$ (solid lines) and $Z = 10^{-4}$ (dashed lines). The lines for low mass WDs truncate at $10^{-8}\,M_\odot$/yr, since the lower boundary of the steady burning regime of these white dwarfs is located between $10^{-8}\,M_\odot$/yr and $10^{-7}\,M_\odot$/yr. In the middle panel, the models with $M_{\rm ej}$=0 are not plotted. (For M_{WD}=0.6 $M_\odot$ and $\dot{M}$=10^{-9} and $10^{-10}\,M_\odot$/yr the models did not reach a steady state and L_{max} is not well defined).

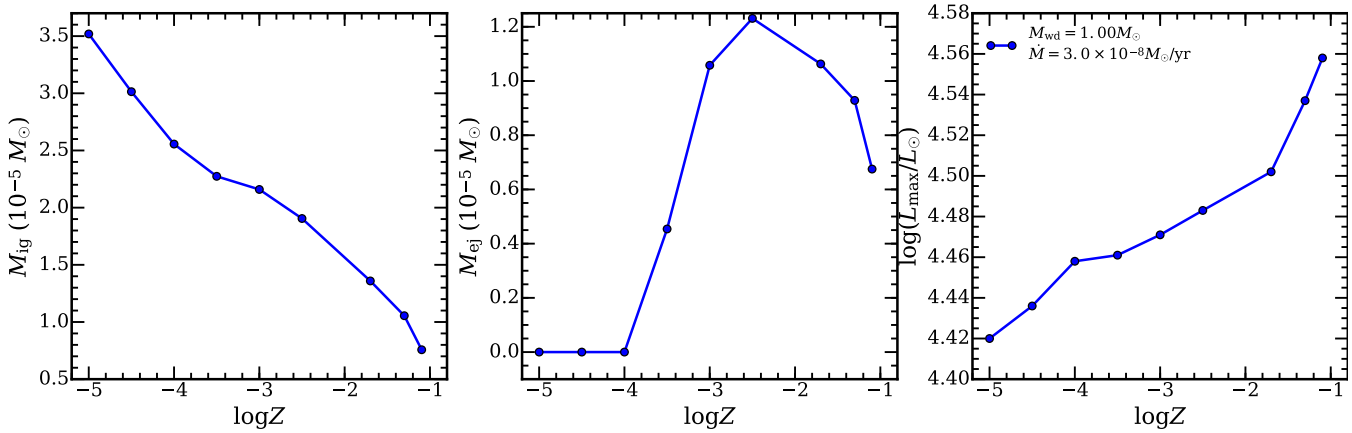


Figure 7. Dependence of nova properties on the metallicity for the white dwarf mass M_{WD}= 1.00 $M_\odot$ and accretion rate $\dot{M} = 3.0 \cdot 10^{-8}\,M_\odot$/yr. In these calculations, we do not take mixing into account. The initial abundance of accreted matter is computed as we describe in Sec. 2.2.

the Eddington luminosity and M_{ej}=0 (Table A4). Evidently, for similar values of $\dot{M}_{accr}$, the recurrence periods of models with low Z are larger than for models with high Z.

In order to understand the dependence of nova properties on metallicity more comprehensively, we computed the evolution of accreting WDs for M_{WD}= 1.00 $M_\odot$ and $\dot{M} = 3.0 \cdot 10^{-8}$ $M_\odot$/yr for a more detailed grid of Z between 10^{-5} and 0.08. For these models, we have computed a large number of outburst cycles in order to be sure that a regular cyclic pattern is obtained. Figure 7 shows the dependence of novae properties on metallicity. It is clear that accreting WDs with smaller metallicities have larger ignition mass and smaller maximum luminosity, as explained above. However, the dependence of M_{ej} on Z is not monotonic. For $Z \lesssim 0.003$, the ejected mass becomes larger for higher metallicity. The reason is the following: on one hand, the nuclear luminosity increases as the metallicity increases, hence the ejected mass increases as the metallicity increases if $Z \lesssim 0.003$; on the other hand, mass loss occurs at smaller photospheric radii as the luminosity increases. Hence, the escape velocity becomes larger, leading to the decrease of M_{ej}. For the lowest Z, luminosity never exceeds L_{Edd} and by virtue of Eq. (2), outbursts do not result in mass-loss.

4.2 Influence of mixing process

In Fig. 8, the properties of models with and without mixing are compared. In the models which include our "mixing" approximation, the metallicity of the H-shell is greater, therefore the differences between the models with and without mixing are similar to the differences between models with high and low metallicity. Thus, for the same reasons as presented in the previous subsection, M_{ign}, M_{ej}, and P_{rec} are smaller in the models which include mixing than in the models without mixing, and the maximum luminosity is larger in the models with mixing. Note that the behaviour of L_{max} in models with mixing (the rightmost panel of Fig. 8) follows an irregular pattern. While the origin of this behaviour is unclear at present, we speculate that it may arise due to the interplay between the rate of energy release, the rate of energy transfer to the surface by convection for outbursts of different strength, and the implemented mass-loss algorithm.

4.3 Dependence of retention efficiency on metallicity and mixing

In Fig. 9, we show the retention efficiency (Eq. (1)) found for different WD masses, accretion rates, and metallicities. We find that the retention efficiency is higher in models with lower metallicity, less massive WDs or higher accretion rates. For more massive WDs or low accretion rates, the degeneracy in the H-layer is higher. For higher metallicity, the nuclear energy production is higher. These circumstances lead to more violent outbursts and lower retention efficiency.

Figure 10 demonstrates the retention efficiency found for our models of a 1.0 $M_\odot$ WD with accretion rate $\dot{M} = 3.0 \times 10^{-8}$ $M_\odot$/yr and different metallicities. This plot clearly shows that retention efficiency decreases with increasing metallicity.

Figure 11 shows the retention efficiency for WDs with different masses, with and without mixing. Note that the solid line for 1.20 $M_\odot$ in the figure intersects other lines, due to numerical noise. We find that the retention efficiency varies for different outbursts and the novae properties do not converge to an asymptotic limit for our models with the lowest accretion rates. In the mixing case the retention efficiency is mostly negative because, as discussed in § 3.3 (see Eq. (3)), the mass involved in the TNR is a factor 4/3 larger than the mass accreted during a full nova cycle M_{acc}. This implies that, except in models with high accretion rates, the C/O enhancement in the accreted layers determines a secular reduction of the underlying WD mass. When comparing our results with those by Yaron et al. (2005), we find that for low values of $\dot{M}$ our estimated retention efficiencies are lower. This indicates that the C/O enrichment we adopted is definitively larger than that enabled by diffusion.

4.4 Influence of different mass loss algorithms

As discussed above, there exist several algorithms in the literature for prescribing mass loss in hydrostatic models of outbursts from accreting WDs. In order to evaluate the effect of different mass loss prescriptions on our results, we carried out trial computations using an alternative simple model in which it is assumed that expanding WD experiences Roche lobe overflow. We computed models of 0.60 $M_\odot$ and 1.0 $M_\odot$ WDs with $Z = 10^{-4}$ which accrete un-enriched matter at different rates. Roche lobe radii were set to 0.2, 0.4, and 1.0 $R_\odot$. Necessarily, these models are not entirely self-consistent, e.g., in any given cataclysmic variable, the mass of the WD, Roche lobe radius, and accretion rate are interrelated via the evolutionary state of the binary, while in symbiotic binaries the notion of a Roche lobe radius is hardly applicable to outbursting WDs. These results are therefore only intended for a qualitative comparison with our models.

The results of these trial computations are presented in Fig. 12. For M_{WD}=0.6 $M_\odot$, WD outbursts never result in mass ejection if the SEW algorithm is assumed. For the RLOF algorithm, however, we find that outbursts may result in the loss of up to (70-80)% of the accreted mass, depending on their strength. Comparing Figs. 9 and 12, we see that for M_{WD}=1 $M_\odot$ the retention efficiency in the SEW case may be slightly higher than in RLOF case, indicating that SEWs remove most of the mass before RLOF. A similar relation between these two algorithms was demonstrated by Wolf et al. (2013) for WDs accreting solar metallicity matter. This inference is confirmed by a computation of a sequence of models for 1 $M_\odot$ WD, in which both SEWs and RLOF were taken into account (for a Roche lobe radius of 0.4 $R_\odot$): in this particular case, the difference in $\log(\eta)$ did not exceed 0.04dex. From Figure 12, however, we may conclude that differing assumptions made in the literature regarding the dominant mechanism driving mass loss in nova eruptions may result in retention efficiencies differing by up to factor $\lesssim 4$, depending on the mass of the accretor, the mass transfer rate, and the dimensions of the system. In light of this analysis, it is clear that the mass-loss algorithm assumed in hydrostatic models remains a critical uncertain parameter in modelling nova eruptions and populations of cataclysmic variables.

This conclusion is confirmed by results of Starrfield (2017), who compared retention efficiency η for 1.35$M_\odot$ WD accreting solar composition matter at a rate of 1.6×10^{-9} $M_\odot$ yr^{-1} assuming three different mass loss prescriptions: SEW, RLOF and ejection of matter that exceeded the escape velocity and became optically thin (Starrfield et al. 2009) . They show that the values of η associated with SEW and RLOF mechanism are quite compatible, while the latter mechanism provides retention efficiency higher by a large factor (up to ~ 6).

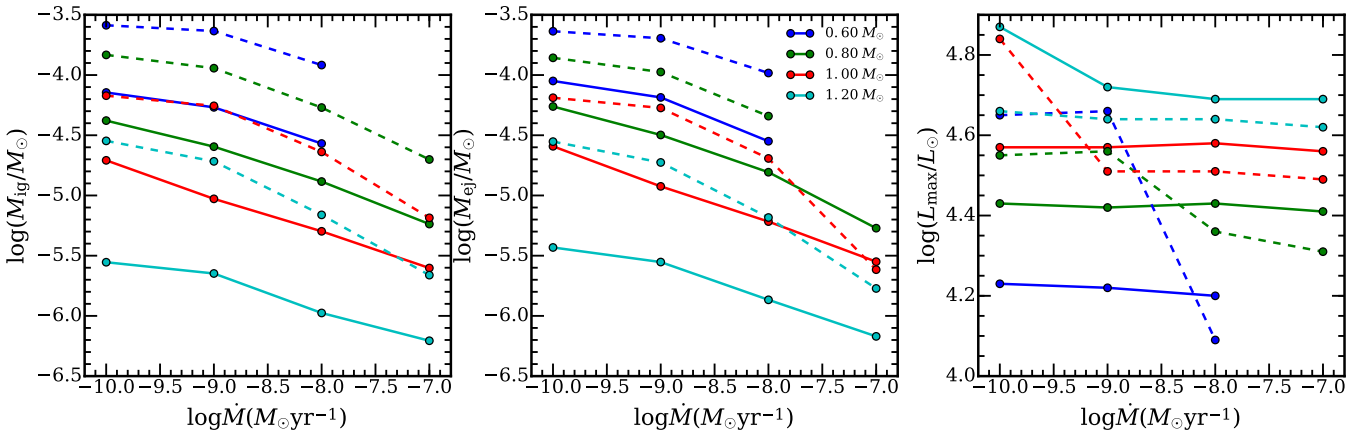


Figure 8. Comparison of models with $Z = 0.02$ with mixing (solid line) and without it (dashed line).

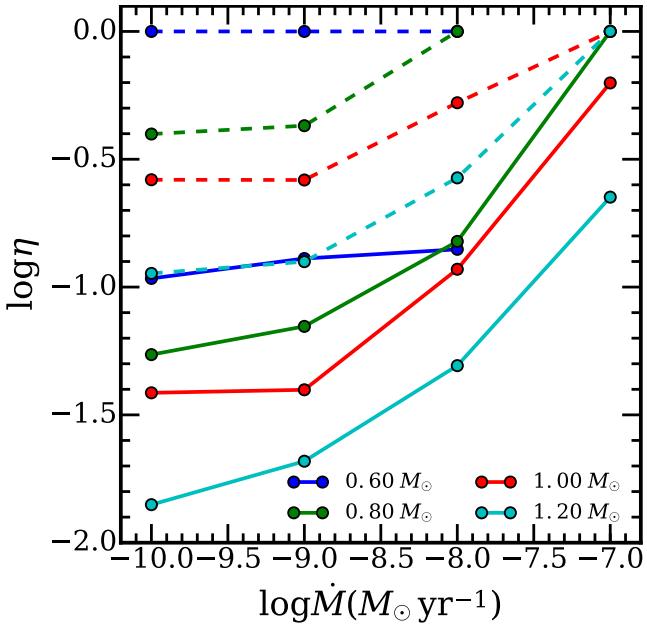


Figure 9. Comparison of retention efficiency for models with $Z = 0.02$ (solid line) and 10^{-4} (dashed line), without mixing. In the models with $Z = 10^{-4}$ and M_{WD}= 0.60 $M_\odot$ luminosity during novae outbursts never exceeds Eddington luminosity.

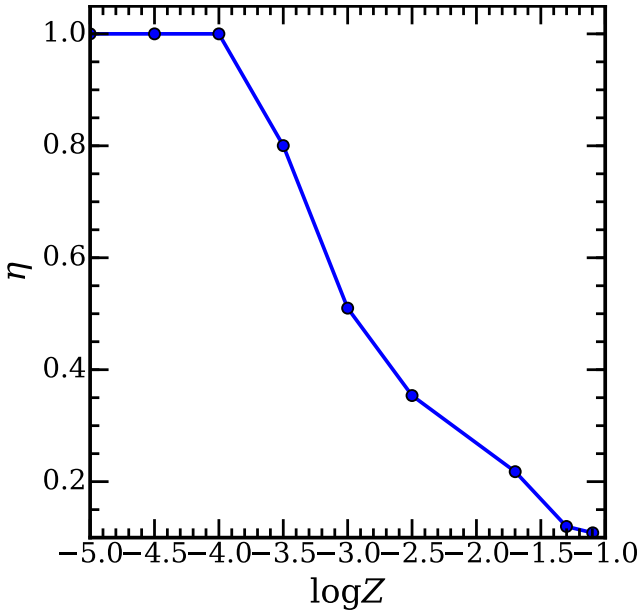


Figure 10. Dependence of retention efficiency on metallicity for 1.0 $M_\odot$ WD with accretion rate $\dot{M} = 3.0 \cdot 10^{-8}\ M_\odot$/yr. In these calculations, we do not take mixing into account.

4.5 Implications for populations of accreting WDs and SNe Ia

In modelling populations of SNe Ia progenitors in the single-degenerate (SD) scenario, among the key ingredients are the location and the breadth of the stability strip in the $M_{WD} - \dot{M}$ plane and efficiency of mass retention by accreting WDs in the unstable nuclear burning regime. Significantly differing results have been obtained by different authors, however, primarily due to differing prescriptions for enrichment and mass-loss. As a result, the delay-time distributions and rates found for SNe Ia in the SD-scenario vary substantially, even for solar Z (see, e.g., Bours et al. 2013).

In our analysis above, we found that location of the boundary of stable nuclear burning and the retention efficiency strongly depend on composition, thus influencing the rate of SNe Ia in the SD-scenario in stellar populations with different metallicities. Additionally, we found that the retention efficiency can be negative for a wide range of accretion rates and WD masses, when enrichment of the accreted matter via mixing with the underlying WD is taken into account. Leaving aside outstanding uncertainties in the physical mechanism(s) driving mass-loss (as discussed above), we note that metallicity may have an important effect not only for hypothetical precursors of SNe Ia, but also for models of other populations of accreting WD binaries, such as cataclysmic variables and symbiotic binaries. These speculations must be verified by future binary population synthesis studies.

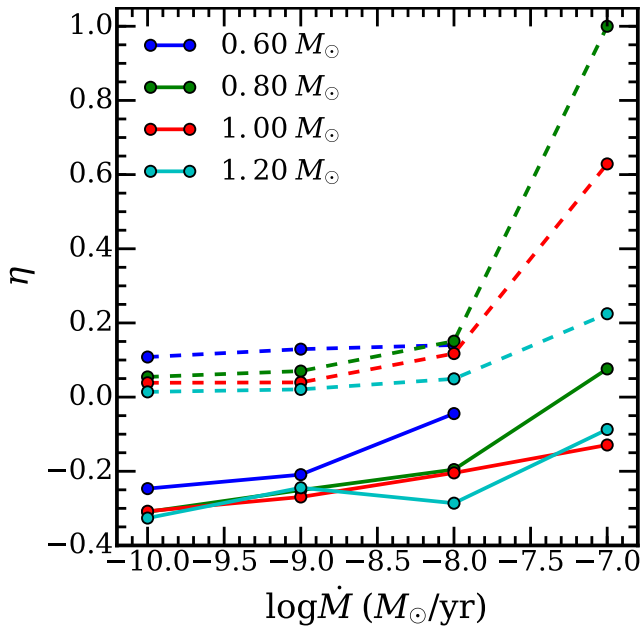


Figure 11. Comparison of retention efficiency for models with $Z = 0.02$, mixing (solid line) and no mixing (dashed line).

5 SUMMARY AND CONCLUSION

Using the publicly-available stellar evolution code MESA, we modelled the evolution of accreting WDs with metallicity $Z = 0.02$ and $Z = 10^{-4}$. White dwarf masses ranged from 0.51 $M_\odot$ to 1.30 $M_\odot$ and accretion rates ranged from 10^{-10} $M_\odot$/yr to 10^{-6} $M_\odot$/yr. For each model, we computed the evolution of accreting WDs with and without a simplified approximation for mixing accreted matter with C/O from the underlying WD. We have investigated the properties of novae in different models as well as the influence of metallicity and mixing on them. We use a mixing fraction of 0.25, close to the upper limit suggested by observations, in order to test the maximum effect that mixing may have upon novae explosions. The main results are as follows:

1) We calculated the range of accretion rates allowing stable H-burning for WDs with $Z = 0.02$ and $Z = 10^{-4}$ (see Fig. 1). For $Z = 10^{-4}$ these rates are lower compared to $Z = 0.02$.

2) For both values of metallicity we computed the key properties of novae (i.e. ignition mass, ejected mass, maximum luminosity) for a comprehensive grid of accreting WDs with different WD masses, accretion rates and metallicities, see Tables A3, A4, A5,A6.

3) We confirm that metallicity has an important impact on the properties of novae. For models with $Z = 0.02$, the ignition masses and recurrence periods are smaller, while the ejected mass and maximum luminosity are larger in contrast to models with $Z = 10^{-4}$. We find that retention efficiency during novae outbursts decreases with increasing metallicity.

4) We remark that in mixing models, by virtue of Eq. (3), at the onset of the first TNR, abundance of metals in the mixed envelope of WD is

$$Z_{env} = (1/3M_{acc}Z_{WD} + M_{acc}Z_\odot)/M_{ign} = 0.265,$$

while $X_{env} = 0.525$, $Y_{env} = 0.21$. Thus, after completion of an outburst cycle, if the ejected mass $M_{\rm ej}$ is lower than $M_{\rm ign}$ as defined in Eq. 3, the surface of the WD should be represented by a He-rich layer having $Y = 0.735$ and $Z = 0.265$, the latter including CNO isotopes, with relative abundances determined by H-burning during the TNR, and original scaled solar mass fraction of other metals. After the beginning of a new cycle, accreted matter with $Z_\odot$ should mix with the matter that has $Z < Z_{WD}$ and mass fraction of metals in the H-rich envelope of the WD at the onset of TNR should reduce, while abundance of He should increase, as compared to the previous outburst. Thus, outburst by outburst, the metals in He+metals layer should become diluted on a pace set by the mass retained in subsequent outbursts. These considerations seem to suggest that in mixing models successive H-flashes have decreasing strength as a lower C/O abundance is dredged-up so that the corresponding retention efficiency should increase. This also implies that a He-buffer massive enough is accumulated, and when it exceeds a crit-

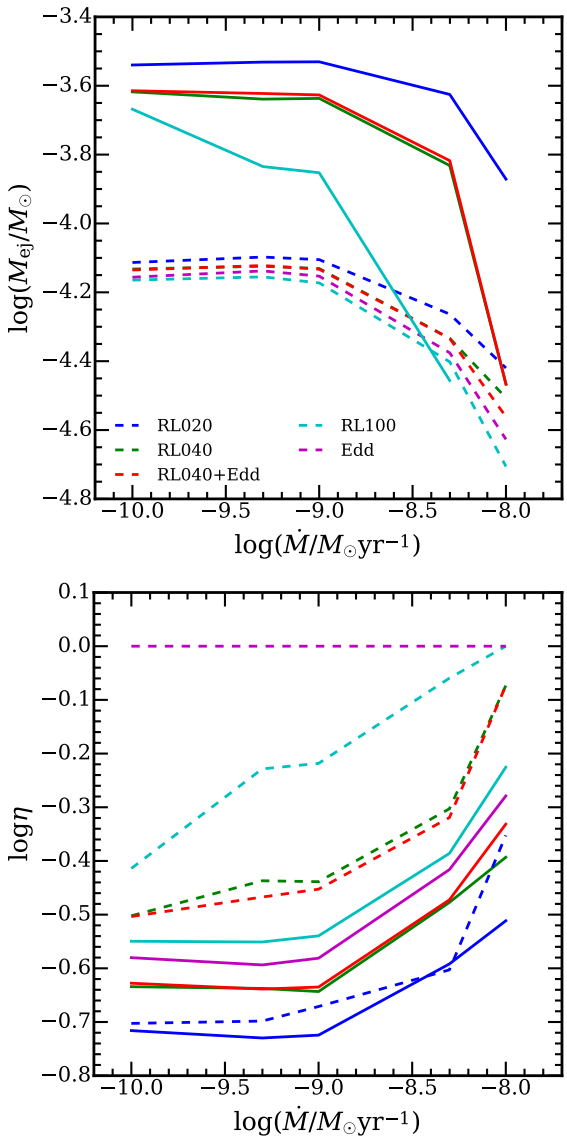


Figure 12. Comparison of ejected mass (upper panel) and retention efficiency (lower panel) for an accreting 0.60 $M_\odot$ (dashed lines) and 1.0 $M_\odot$ (solid lines) WD with different mass loss prescriptions, i.e. super-Eddington wind and Roche lobe overflow at $Z = 10^{-4}$ without mixing. Three constant values of Roche lobe radii were assumed: 0.2, 0.4, and 1.0 $R_\odot$. The model with $M_{\rm WD} = 0.60$ $M_\odot$ under assumption of super-Eddington wind only does not eject mass and it is not plotted in the upper panel.

ical value depending on the WD total mass and the effective mass deposition rate, a He-flash occurs.

5) For our low-metallicity models, we found that the super-Eddington wind prescription for mass loss by low-mass WDs results in 100% retention efficiency η (at least for $0.6\,M_\odot$ WDs), while it may be as low as 20% if the RLOF prescription is applied. This depends, however, on the dimensions of the Roche lobe in a particular binary. For high-mass WDs ($1\,M_\odot$), the SEW and RLOF prescriptions result in comparable η for weak outbursts, but may differ by about $\Delta\log(\eta) \sim 0.1$ in either direction, depending on the dimensions of the Roche lobe. Finding of actual mass-loss algorithm and its efficiency is one of the most acute problems, which hamper modelling of stellar populations with accreting WDs like CVs or solving the problem of significance of single-degenerate channel for SNe Ia.

6 ACKNOWLEDGEMENTS

The authors gratefully acknowldge insightful comments by the anonymous referee which helped to improve the paper. HLC would like to thank Bill Wolf for helpful discussions about MESA calculation and Xiangcun Meng for helpful discussion about the influence of metallicity. We also would like to thank Hans Ritter for helpful discussions on novae at low metallicity and Oscar Straniero for discussion on chemical composition of WDs at different metallicities. We are grateful to the MESA council for the Mesa instrument papers and website. This work is partially supported by the National Natural Science Foundation of China (Grants no. 11703081,11521303,11733008), Yunnan Province (No. 2017HC018) and the CAS light of West China Program, Youth Innovation Promotion Association of Chinese Academy of Sciences (Grant no. 2018076). This work was partially supported by Basic Research Program P-28 of the Presidium of the Russian Academy of Sciences and RFBR grant No. 19-02-00790. HLC, LRY, TEW gratefully acknowledge warm hospitality and support of MPA-Garching. MG acknowledges hospitality of Kazan Federal University (KFU) and support by the Russian Government Program of Competitive Growth of KFU. HLC acknowledges the computing time granted by the Yunnan Observatories and provided on the facilities at the Yunnan Observatories Supercomputing Platform.

REFERENCES

Bode M. F., Evans A., 2008, Classical Novae
Bours M. C. P., Toonen S., Nelemans G., 2013, A&A, 552, A24
Casanova J., José J., García-Berro E., Calder A., Shore S. N., 2010, A&A, 513, L5
Casanova J., José J., García-Berro E., Shore S. N., 2016, A&A, 595, A28
Casanova J., José J., Shore S. N., 2018, A&A, 619, A121
Cassisi S., Iben Jr. I., Tornambe A., 1998, ApJ, 496, 376
Chen H.-L., Woods T. E., Yungelson L. R., Gilfanov M., Han Z., 2016, MNRAS, 458, 2916
Curtin C., Shafter A. W., Pritchet C. J., Neill J. D., Kundu A., Maccarone T. J., 2015, ApJ, 811, 34
Della Valle M., 2002, in Hernanz M., José J., eds, American Institute of Physics Conference Series Vol. 637, Classical Nova Explosions. pp 443–456 (arXiv:astro-ph/0210276), doi:10.1063/1.1518244
Denissenkov P. A., Herwig F., Bildsten L., Paxton B., 2013, ApJ, 762, 8
Denissenkov P. A., Herwig F., Battino U., Ritter C., Pignatari M., Jones S., Paxton B., 2017, ApJ, 834, L10
Doherty C. L., Gil-Pons P., Siess L., Lattanzio J. C., Lau H. H. B., 2015, MNRAS, 446, 2599
Fujimoto M. Y., 1982, ApJ, 257, 767
Fujimoto M. Y., Taam R. E., 1982, ApJ, 260, 249
Gehrz R. D., Truran J. W., Williams R. E., Starrfield S., 1998, PASP, 110, 3
Gilfanov M., Bogdán Á., 2010, Nature, 463, 924
Glasner S. A., Livne E., 1995, ApJ, 445, L149
Glasner S. A., Livne E., Truran J. W., 2012, MNRAS, 427, 2411
Graur O., Woods T. E., 2019, MNRAS, 484, L79
Hachisu I., Kato M., Nomoto K., 1996, ApJ, 470, L97
Hernanz M., Jose J., Coc A., Isern J., 1996, ApJ, 465, L27
Hillman Y., Orio M., Prialnik D., Shara M., Bezák P., Dobrotka A., 2019, ApJ, 879, L5
Iben Jr. I., 1982, ApJ, 259, 244
Iben Icko J., 1988, ApJ, 324, 355
Johansson J., Woods T. E., Gilfanov M., Sarzi M., Chen Y.-M., Oh K., 2016, MNRAS, 461, 4505
José J., 2014, in Woudt P. A., Ribeiro V. A. R. M., eds, Astronomical Society of the Pacific Conference Series Vol. 490, Stellar Novae: Past and Future Decades. p. 275
José J., García-Berro E., Hernanz M., Gil-Pons P., 2007, ApJ, 662, L103
Kato M., 1997, ApJS, 113, 121
Kato M., Hachisu I., Henze M., 2013, ApJ, 779, 19
Kelly K. J., Iliadis C., Downen L., José J., Champagne A., 2013, ApJ, 777, 130
Kuuttila J., Gilfanov M., Seitenzahl I. R., Woods T. E., Vogt F. P. A., 2019, MNRAS, 484, 1317
Livio M., Truran J. W., 1994, ApJ, 425, 797
Livio M., Shankar A., Burkert A., Truran J. W., 1990, ApJ, 356, 250
Lodders K., 2003, ApJ, 591, 1220
Ma X., Chen X., Chen H.-L., Denissenkov P. A., Han Z., 2013, ApJ, 778, L32
MacDonald J., 1984, ApJ, 283, 241
Maccarone T. J., et al., 2019, arXiv e-prints, p. arXiv:1907.02130
Maoz D., Mannucci F., Nelemans G., 2014, ARA&A, 52, 107
Nomoto K., Nariai K., Sugimoto D., 1979, PASJ, 31, 287
Paczynski B., Proszynski M., 1986, ApJ, 302, 519
Paczynski B., Zytkow A. N., 1978, ApJ, 222, 604
Paxton B., Bildsten L., Dotter A., Herwig F., Lesaffre P., Timmes F., 2011, ApJS, 192, 3
Paxton B., et al., 2013, ApJS, 208, 4
Paxton B., et al., 2015, ApJS, 220, 15
Piersanti L., Cassisi S., Iben Jr. I., Tornambé A., 2000, ApJ, 535, 932
Politano M., Starrfield S., Truran J. W., Weiss A., Sparks W. M., 1995, ApJ, 448, 807
Pols O. R., Schröder K.-P., Hurley J. R., Tout C. A., Eggleton P. P., 1998, MNRAS, 298, 525
Postnov K. A., Yungelson L. R., 2014, Living Reviews in Relativity, 17, 3
Prialnik D., 1986, ApJ, 310, 222
Prialnik D., 1987, Ap&SS, 131, 431
Prialnik D., Kovetz A., 1995, ApJ, 445, 789
Quataert E., Fernández R., Kasen D., Klion H., Paxton B., 2016, MNRAS, 458, 1214
Quinn T., Paczynski B., 1985, ApJ, 289, 634
Ritter H., 1990, in Cassatella A., Viotti R., eds, Lecture Notes in Physics, Berlin Springer Verlag Vol. 369, IAU Colloq. 122: Physics of Classical Novae. p. 313, doi:10.1007/3-540-53500-4_144
Ritter H., Kolb U., 2011, VizieR Online Data Catalog, 1
Schatzman E., 1963, in L. Gratton ed., Star Evolution. pp 389–+
Shafter A. W., 2017, ApJ, 834, 196
Shafter A. W., Curtin C., Pritchet C. J., Bode M. F., Darnley M. J., 2014, in Woudt P. A., Ribeiro V. A. R. M., eds, Astronomical Society of the Pacific Conference Series Vol. 490, Stellar Novae: Past and Future Decades. p. 77 (arXiv:1307.2296)
Shara M. M., Drissen L., 1995, ApJ, 448, 203
Shara M. M., Prialnik D., Shaviv G., 1977, A&A, 61, 363
Shaviv N. J., 2002, in Hernanz M., José J., eds, American Institute of Physics Conference Series Vol. 637, Classical Nova Explosions. pp

259–265 (arXiv:astro-ph/0207639), doi:10.1063/1.1518210
Shen K. J., Bildsten L., 2007, ApJ, 660, 1444
Soraisam M. D., Gilfanov M., 2015, A&A, 583, A140
Starrfield S., 2017, Evolution of Accreting White Dwarfs to the Thermonuclear Runaway. p. 1211, doi:10.1007/978-3-319-21846-5_59
Starrfield S., Truran J. W., Sparks W. M., 1978, ApJ, 226, 186
Starrfield S., Sparks W. M., Shaviv G., 1988, ApJ, 325, L35
Starrfield S., Schwarz G., Truran J. W., Sparks W. M., 2000, in Holt S. S., Zhang W. W., eds, American Institute of Physics Conference Series Vol. 522, American Institute of Physics Conference Series. pp 379–382, doi:10.1063/1.1291739
Starrfield S., Iliadis C., Hix W. R., Timmes F. X., Sparks W. M., 2009, ApJ, 692, 1532
Starrfield S., Iliadis C., Hix W. R., 2016, PASP, 128, 051001
Starrfield S., Bose M., Iliadis C., Hix W. R., Wagner R. M., Woodward C. E., Jose J., Hernanz M., 2017, in The Golden Age of Cataclysmic Variables and Related Objects IV. p. 66
Townsley D. M., Bildsten L., 2004, ApJ, 600, 390
Truran J. W., Cameron A. G. W., 1971, Ap&SS, 14, 179
Truran J. W., Livio M., 1986, ApJ, 308, 721
Umeda H., Nomoto K., Yamaoka H., Wanajo S., 1999, ApJ, 513, 861
Wang B., 2018, Research in Astronomy and Astrophysics, 18, 049
Warner B., 2003, Cataclysmic Variable Stars. Cambridge University Press
Wolf W. M., Bildsten L., Brooks J., Paxton B., 2013, ApJ, 777, 136
Woods T. E., Gilfanov M., 2014, MNRAS, 439, 2351
Woods T. E., Ghavamian P., Badenes C., Gilfanov M., 2017, Nature Astronomy, 1, 800
Woods T. E., Ghavamian P., Badenes C., Gilfanov M., 2018, ApJ, 863, 120
Yaron O., Prialnik D., Shara M. M., Kovetz A., 2005, ApJ, 623, 398

APPENDIX A: STEADY BURNING BOUNDARIES FOR $Z = 0.02$ AND $Z = 10^{-4}$

In table A1 and A2, we present the steady burning boundaries for different WD mass at $Z = 0.02$ and $Z = 10^{-4}$.

Fitting formulae for the boundaries of steady-burning zones are given by the following formulae. These formulae desire the numerical results with the accuracy of better than 0.3%.
For $Z = 0.02$:

$$\log(\dot{M}_{\rm lower}) = -10.35 + 8.37 \cdot M_{\rm WD} - 6.84 \cdot M_{\rm WD}^2 + 2.07 \cdot M_{\rm WD}^3 \quad \text{(A1)}$$

$$\log(\dot{M}_{\rm upper}) = -9.30 + 6.72 \cdot M_{\rm WD} - 5.28 \cdot M_{\rm WD}^2 + 1.50 \cdot M_{\rm WD}^3 \quad \text{(A2)}$$

For $Z = 10^{-4}$:

$$\log(\dot{M}_{\rm lower}) = -12.21 + 13.32 \cdot M_{\rm WD} - 11.90 \cdot M_{\rm WD}^2 + 3.82 \cdot M_{\rm WD}^3 \quad \text{(A3)}$$

$$\log(\dot{M}_{\rm upper}) = -9.81 + 7.25 \cdot M_{\rm WD} - 5.17 \cdot M_{\rm WD}^2 + 1.32 \cdot M_{\rm WD}^3 \quad \text{(A4)}$$

Table A1. Steady burning boundaries for $Z = 0.02$. The first column is the WD mass; The second and third columns are the lower and upper boundaries, respectively.

M_{WD} ($M_\odot$)	$\dot{M}_{lower}(M_\odot/yr)$	$\dot{M}_{upper}(M_\odot/yr)$
0.51	0.25e-7	0.88e-7
0.60	0.47e-7	1.42e-7
0.70	0.73e-7	2.14e-7
0.80	1.04e-7	2.86e-7
0.90	1.37e-7	3.56e-7
1.00	1.73e-7	4.26e-7
1.10	2.19e-7	4.96e-7
1.20	2.65e-7	5.60e-7
1.30	3.21e-7	6.24e-7

Table A2. Steady burning boundaries for $Z = 10^{-4}$. The first column is the WD mass; The second and third columns are the lower and upper boundaries, respectively.

M_{WD} ($M_\odot$)	$\dot{M}_{lower}(M_\odot/yr)$	$\dot{M}_{upper}(M_\odot/yr)$
0.51	9.8e-9	5.12e-8
0.60	2.13e-8	9.36e-8
0.70	4.1e-8	1.55e-7
0.80	6.0e-8	2.18e-7
0.90	8.2e-8	3.02e-7
1.00	1.07e-7	4.08e-7
1.10	1.39e-7	4.54e-7
1.20	1.74e-7	5.34e-7
1.30	2.42e-7	6.01e-7

Table A3. Characteristics of nova outburst without mixing for solar metallicities.

M_{wd} ($M_\odot$)	$\dot{M}_{acc}$ ($\dot{M}_\odot$/yr)	Number of outburst computed	M_{acc} ($M_\odot$)	M_{ej} ($M_\odot$)	logL_{max} ($L_\odot$)
0.51	1.0e-10	3	3.46e-4	1.22e-4	4.06
0.51	1.0e-9	5	2.71e-4	1.21e-4	4.06
0.51	1.0e-8	29	1.57e-4	1.13e-4	3.90
0.60	1.0e-10	1	2.59e-4	2.31e-4	4.65
0.60	1.0e-9	11	2.32e-4	2.02e-4	4.66
0.60	1.0e-8	72	1.21e-4	1.04e-4	4.09
0.70	1.0e-10	7	2.02e-4	1.89e-4	4.54
0.70	1.0e-9	18	1.64e-4	1.51e-4	4.66
0.70	1.0e-8	145	8.51e-5	7.00e-5	4.23
0.80	1.0e-10	4	1.47e-4	1.39e-4	4.55
0.80	1.0e-9	11	1.14e-4	1.06e-4	4.56
0.80	1.0e-8	154	5.37e-5	4.56e-5	4.36
0.80	1.0e-7	241	1.99e-5	0.00	4.31
0.90	1.0e-10	12	1.09e-4	1.05e-4	4.70
0.90	1.0e-9	12	7.73e-5	7.31e-5	4.57
0.90	1.0e-8	134	3.61e-5	3.09e-5	4.43
0.90	1.0e-7	233	1.09e-5	0.000	4.41
1.00	1.0e-10	5	6.74e-5	6.48e-5	4.84
1.00	1.0e-9	32	5.55e-5	5.33e-5	4.51
1.00	1.0e-8	125	2.30e-5	2.03e-5	4.51
1.00	1.0e-7	217	6.52e-6	2.42e-6	4.49
1.10	1.0e-10	2	4.25e-5	4.16e-5	4.71
1.10	1.0e-9	37	3.53e-5	3.44e-5	4.58
1.10	1.0e-8	102	1.41e-5	1.32e-5	4.58
1.10	1.0e-7	32	3.91e-6	2.75e-6	4.56
1.20	1.0e-10	1	2.84e-5	2.80e-5	4.66
1.20	1.0e-9	19	1.92e-5	1.88e-5	4.64
1.20	1.0e-8	61	6.90e-6	6.56e-6	4.64
1.20	1.0e-7	78	2.18e-6	1.69e-6	4.62
1.30	1.0e-10	1	1.48e-5	1.47e-5	5.20
1.30	1.0e-9	24	7.53e-6	7.24e-6	4.75
1.30	1.0e-8	109	2.53e-6	2.30e-6	4.72
1.30	1.0e-7	286	8.03e-7	6.13e-7	4.70

Table A4. Characteristics of nova outburst without mixing for $Z = 0.0001$.

$M_{\rm wd}$ ($M_\odot$)	$\dot{M}_{\rm acc}$ ($\dot{M}_\odot$/yr)	Number of outburst computed	$M_{\rm acc}$ ($M_\odot$)	$M_{\rm ej}$ ($M_\odot$)	log$L_{\rm max}$ ($L_\odot$)
0.51	1.0e-10	93	4.28e-4	0.000	3.78
0.51	1.0e-9	39	4.53e-4	0.000	3.76
0.60	1.0e-10	108	3.42e-4	0.000	3.98
0.60	1.0e-9	18	3.45e-4	0.000	3.96
0.60	1.0e-8	177	2.16e-4	0.000	3.92
0.70	1.0e-10	13	2.59e-4	1.27e-4	4.16
0.70	1.0e-9	19	2.58e-4	7.36e-5	4.14
0.70	1.0e-8	65	1.47e-4	0.00	4.11
0.80	1.0e-10	13	1.94e-4	1.17e-4	4.27
0.80	1.0e-9	17	1.94e-4	1.11e-4	4.26
0.80	1.0e-8	43	1.04e-4	0.00	4.24
0.90	1.0e-10	64	1.36e-4	8.69e-5	4.38
0.90	1.0e-9	17	1.37e-4	8.68e-5	4.37
0.90	1.0e-8	140	7.24e-5	2.63e-5	4.36
1.00	1.0e-10	64	9.47e-5	6.98e-5	4.46
1.00	1.0e-9	10	9.53e-5	7.03e-5	4.46
1.00	1.0e-8	52	4.98e-5	2.36e-5	4.45
1.00	1.0e-7	79	1.62e-5	0.00	4.40
1.10	1.0e-10	9	6.36e-5	5.24e-5	4.54
1.10	1.0e-9	30	6.24e-5	5.14e-5	4.54
1.10	1.0e-8	24	3.17e-5	1.98e-5	4.53
1.10	1.0e-7	41	8.61e-6	0.00	4.50
1.20	1.0e-10	39	3.89e-5	3.45e-5	4.62
1.20	1.0e-9	28	3.58e-5	3.13e-5	4.61
1.20	1.0e-8	56	1.72e-5	1.26e-5	4.61
1.20	1.0e-7	123	4.12e-6	0.00	4.58
1.30	1.0e-10	2	1.93e-5	1.85e-5	4.74
1.30	1.0e-9	20	1.83e-5	1.66e-5	4.70
1.30	1.0e-8	63	6.92e-6	5.73e-6	4.70
1.30	1.0e-7	84	1.43e-6	2.18e-7	4.67

Table A5. Characteristics of nova outburst with mixing for solar metallicities.

$M_{\rm wd}$ ($M_\odot$)	$\dot{M}_{\rm acc}$ ($\dot{M}_\odot$/yr)	number of outburst computed	$M_{\rm acc}$ ($M_\odot$)	$M_{\rm ej}$ ($M_\odot$)	log$L_{\rm max}$ ($L_\odot$)
0.51	1.0e-10	1	7.10e-5	8.88e-5	4.04
0.51	1.0e-9	46	7.88e-5	9.67e-5	4.22
0.51	1.0e-8	71	4.28e-5	4.63e-5	4.05
0.60	1.0e-10	1	7.16e-5	8.93e-5	4.23
0.60	1.0e-9	36	5.39e-5	6.52e-5	4.22
0.60	1.0e-8	72	2.70e-5	2.82e-5	4.20
0.70	1.0e-10	5	5.99e-5	7.70e-5	4.36
0.70	1.0e-9	33	3.68e-5	4.44e-5	4.34
0.70	1.0e-8	66	1.86e-5	2.01e-5	4.33
0.70	1.0e-7	164	0.83e-5	1.30e-6	4.30
0.80	1.0e-10	4	4.18e-5	5.48e-5	4.43
0.80	1.0e-9	31	2.54e-5	3.18e-5	4.42
0.80	1.0e-8	69	1.30e-5	1.56e-5	4.43
0.80	1.0e-7	136	5.79e-6	5.35e-6	4.41
0.90	1.0e-10	6	2.69e-5	3.56e-5	4.76
0.90	1.0e-9	42	1.79e-5	2.26e-5	4.52
0.90	1.0e-8	65	8.17e-6	9.89e-6	4.50
0.90	1.0e-7	127	3.95e-6	4.21e-6	4.49
1.00	1.0e-10	8	1.96e-5	2.56e-5	4.57
1.00	1.0e-9	21	9.38e-6	1.19e-5	4.57
1.00	1.0e-8	61	5.04e-6	6.07e-6	4.58
1.00	1.0e-7	124	2.49e-6	2.82e-6	4.56
1.10	1.0e-10	7	1.67e-5	2.22e-5	4.64
1.10	1.0e-9	41	6.39e-6	8.32e-6	4.88
1.10	1.0e-8	63	2.64e-6	3.27e-6	4.64
1.10	1.0e-7	99	1.32e-6	1.49e-6	4.63
1.20	1.0e-10	1	2.79e-6	3.70e-6	4.87
1.20	1.0e-9	16	2.25e-6	2.80e-6	4.72
1.20	1.0e-8	24	1.06e-6	1.36e-6	4.69
1.20	1.0e-7	98	6.22e-7	6.76e-7	4.69
1.30	1.0e-10	2	1.02e-6	1.24e-6	4.81
1.30	1.0e-9	11	6.02e-7	6.69e-7	4.78
1.30	1.0e-8	30	3.68e-7	4.11e-7	4.77
1.30	1.0e-7	36	1.86e-7	1.75e-7	4.75

Table A6. Characteristics of nova outburst with mixing for $Z = 0.0001$.

$M_{\rm wd}$ ($M_\odot$)	$\dot{M}_{\rm acc}$ ($\dot{M}_\odot$/yr)	Number of outburst computed	$M_{\rm acc}$ ($M_\odot$)	$M_{\rm ej}$ ($M_\odot$)	log$L_{\rm max}$ $L_\odot$
0.51	1.0e-10	3	1.10e-4	1.21e-4	4.10
0.51	1.0e-9	16	7.31e-5	7.04e-5	4.08
0.51	1.0e-8	48	3.50e-5	1.03e-5	4.06
0.60	1.0e-10	3	0.76e-4	8.66e-5	4.22
0.60	1.0e-9	31	5.35e-5	5.59e-5	4.21
0.60	1.0e-8	36	2.47e-5	1.31e-5	4.20
0.70	1.0e-10	2	4.16e-5	4.70e-5	4.33
0.70	1.0e-9	32	3.48e-5	3.79e-5	4.34
0.70	1.0e-8	35	1.74e-5	1.34e-5	4.33
0.70	1.0e-7	94	9.23e-6	0.00	4.30
0.80	1.0e-10	12	5.17e-5	6.64e-5	4.43
0.80	1.0e-9	18	3.34e-5	4.41e-5	4.63
0.80	1.0e-8	41	1.28e-5	1.25e-5	4.42
0.80	1.0e-7	121	5.42e-6	0.00	4.40
0.90	1.0e-10	17	4.52e-5	6.01e-5	4.51
0.90	1.0e-9	24	1.44e-5	1.73e-5	4.50
0.90	1.0e-8	89	8.10e-6	9.20e-6	4.52
0.90	1.0e-7	71	3.74e-6	3.16e-6	4.49
1.00	1.0e-10	6	1.69e-5	2.25e-5	4.73
1.00	1.0e-9	20	1.04e-5	1.26e-5	4.59
1.00	1.0e-8	41	5.03e-6	5.80e-6	4.58
1.00	1.0e-7	99	2.42e-6	2.31e-6	4.56
1.10	1.0e-10	8	1.07e-5	1.39e-5	4.67
1.10	1.0e-9	35	5.75e-6	7.39e-6	4.64
1.10	1.0e-8	30	2.96e-6	3.38e-6	4.63
1.10	1.0e-7	20	1.27e-6	1.19e-6	4.62
1.20	1.0e-10	17	2.61e-6	3.22e-6	4.71
1.20	1.0e-9	88	2.06e-6	2.49e-6	4.70
1.20	1.0e-8	86	1.58e-6	1.80e-6	4.69
1.20	1.0e-7	270	7.10e-7	6.82e-7	4.68
1.30	1.0e-10	4	1.69e-6	2.14e-6	4.81
1.30	1.0e-9	31	9.53e-7	1.12e-6	4.78
1.30	1.0e-8	37	5.54e-7	6.04e-7	4.77
1.30	1.0e-7	129	2.42e-7	2.24e-7	4.75

This paper has been typeset from a TEX/LATEX file prepared by the author.